A judging criterion of state-mutation switching cycle for sliding mode controlled non-isolated grid-connection inverter with H6-type

Zichao Guan[1, a, *], Rui Chen[1], Jiajie Li[1] and Xu Gou[2]

[1]School of Southwest Petroleum University, Chengdu, China
[2]School of Chengdu University of Technology, Chengdu, China

[*, a] Corresponding author e-mail: 771378965@qq.com

Abstract. To confirm state-mutation switching cycle of the sliding mode controlled non-isolated grid-connected inverter with H6-type (SMCNGI-H6) system, a novel judging criterion is proposed. With the case of folded diagram, state-mutation phenomenon is observed that the state variable changes from period-1 to period-doubling at a certain switching cycle. Then the root cause of state-mutation phenomenon is explored. Meanwhile, regarding the variation of state-mutation switching cycle with the parameters of sliding mode controller (SMC), a novel criterion is proposed to determine state-mutation switching cycle of the state variable. The numerical simulations and experimental results show that state-mutation switching cycle can be precisely determined by the judging criterion.

1. Introduction

A high efficiency, non-isolated grid-connected inverter with H6-type (NGI-H6) is proposed [1]. Different from the H-bridge grid-connected inverter, this topology embeds two high-performance diodes into the midpoint of a full bridge inverter, which provide freewheel paths and separate the DC power from a grid during freewheeling time [1]. SMC is recognized as a robust controller with fast dynamic response and high stability in a wide range of operating conditions, so it is widely used in the control of inverter [2].

SMC is a nonlinear controller, so the criterions that have to take the derivative of discrete-model equations are unsuitable for the SMC inverter [2]. Bifurcation diagram is a picture of several fixed switching cycles of the state variables under different bifurcation parameters, which needs not to solve the differential discrete-model equations, so it's an efficient criterion to analyse stability domain and bifurcation phenomena in the SMC inverter [2-4].

However, state-mutation phenomenon exists in the SMC inverter, where the state variable changes from period-1 to period-doubling at a certain switching cycle for a specific SMC parameter. Moreover, the state-mutation switching cycle varies with different SMC parameters. If bifurcation diagram of inverter selects state-mutation switching cycle as fixed sample switching cycle, bifurcation diagram can correctly show stability domain and bifurcation phenomena of the SMC inverter [2]-[3]. Thus, the confirmation of state-mutation switching cycle is the key to draw the bifurcation diagram for the SMC inverter. In this paper, a novel criterion to determine the state-mutation switching cycle is proposed and state-mutation phenomenon is analysed with taking SMCNGCI-H6 system as an example.

Content from this work may be used under the terms of the Creative Commons Attribution 3.0 licence. Any further distribution of this work must maintain attribution to the author(s) and the title of the work, journal citation and DOI.
Published under licence by IOP Publishing Ltd

2. State analysis and discretely modelling of SMCNGCI-H6 system

2.1. The operation of SMCNGI-H6 system

Figure 1 shows the SMCNGI-H6 system (system for short). E is DC input voltage E=400V, u_{grid} is grid voltage, u_{grid}=220×sin(2πft)V, f is the frequency of u_{grid} f=50Hz. L-filter is selected, D_1, D_2 are freewheel diodes. R_1, R_2 are the parasitic resistances of filter inductances L_1, L_2. i is the inductance current. i_{ref} is the reference current, i_{ref}=5×sin(2πft)A. $u_{control}$ is modulation signal, $u_{carrier}$ is triangular carrier wave. f_s is switching frequency f_s=5kHz, T_s is switching cycle T_s=1/f_s=200us. Figure 2 shows the driver signals of power switches S_1～S_6 by the single polarity SPWM control criterion. The gate signals of S_1～S_4 are given out by comparing $u_{control}$ and $u_{carrier}$, S_5 and S_6 are given out by comparing $u_{control}$ and zero signal.

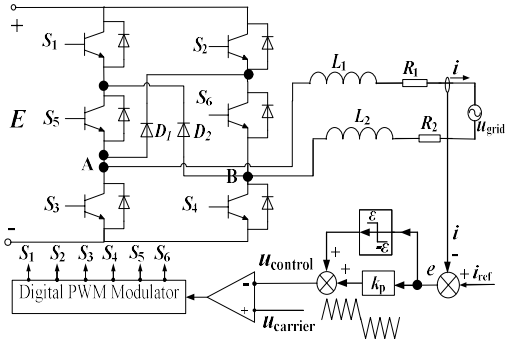


Figure 1. Principle of the SMCNGI-H6 system

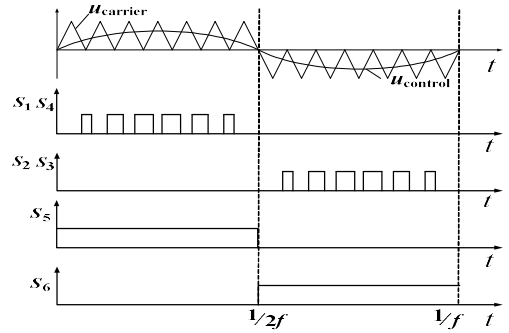


Figure 2. The driver signals of S1～S6 by the single polarity SPWM

As is shown in Figure 1, UAB is the bridge voltage of the NGCI-H6 between point A and B. If i flows from A to B, i is positive. According to the direction of i and conduction conditions of S1～S6, NGCI-H6 can be divided into 4 operating modes.

Operating mode 1: When i>0, S1, S4, S5 turn on and S2, S3, S6 , D1, D2 turn off, the system operates at mode 1. From Figure 1, E, S1, S4, S5, L1, R1, ugrid, L2 and R2 constitute a charging circuit, so UAB is

$$U_{AB} = +E \tag{1}$$

When L_1=L_2=L, R_1=R_2=R, based on Kirchhoff's voltage law, differential equation of operating mode 1 is

$$\frac{di}{dt} = -\frac{R}{L}i + \frac{E}{2L} - \frac{u_{grid}}{2L} \tag{2}$$

The type (2) can also be rewritten as

$$\dot{X} = AX + B_1U \tag{3}$$

Where X=i, A=[-R/L], B_1=[1/(2L), -1/(2L)], U=[E, u_{grid}]^T.

Operating mode 2: When i>0, S_5, D_2 turn on and power switches S_1, S_2, S_3,S_4, S_6, D_1 turn off, the system operates at mode 2. From Figure 1, S_5, L_1, R_1, u_{grid}, L_2, R_2 and D_2 constitute a freewheel circuit. So U_{AB} and state equation of operating mode 2 can be expressed as type (4) and type (5), respectively.

$$U_{AB} = 0 \tag{4}$$

$$\frac{di}{dt} = -\frac{R}{L}i - \frac{u_{grid}}{2L} \tag{5}$$

The type (6) can also be rewritten as

$$\dot{X} = AX + B_2U \tag{6}$$

Where B_2=[0, -1/(2L)]. The analysis of operating mode 3 and mode 4 are similar to mode 1 and mode 2, respectively. Four operating modes can be expressed as four differential equations, which are listed in Table 1, Where B_3=[-1/(2L), -1/(2L)], B_4= B_2=[0, -1/(2L)].

Table 1. Operating modes and state equations of NGCI-H6

operating modes	turn-off switches	turn-on switches	state equations
1	S_2, S_3, S_6, D_1, D_2	S_1, S_4, S_5	$\dot{X} = AX + B_1U$
2	S_1, S_2, S_3, S_4, S_6, D_1	S_5, D_2	$\dot{X} = AX + B_2U$
3	S_1, S_4, S_5, D_1, D_2	S_2, S_3, S_6	$\dot{X} = AX + B_3U$
4	S_1, S_2, S_3, S_4, S_5, D_2	S_6, D_1	$\dot{X} = AX + B_4U$

2.2. The discrete model of SMCNGCI-H6

Based on the stroboscopic map criterion, T_s is considered as stroboscopic sampling interval, the terminal time of state variables i(n+1) is indicated by initial-time of state variables i(n) within the (n)th T_s, where i(n) and i(n+1) are the inductor current at the (n)th T_s and (n+1)th T_s, respectively. The waveforms of i and U_{AB} is shown in Figure 3.

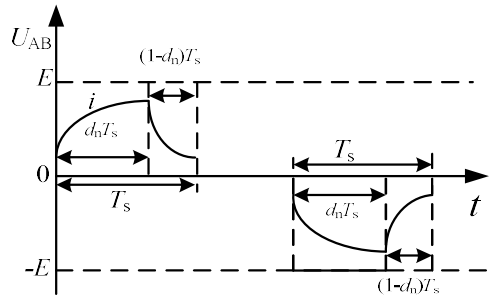


Figure 3. Waveforms of i and UAB with stroboscopic map model

When $i>0$, the system behaves 2 operating modes in a T_s. When $nT_s \le t \le (n+d_n)T_s$, the system works at mode 1. From Figure.1, L_1 and L_2 are charged by the DC-power E, and from Figure.3, i rises. The iteration relations of $X(n)$ and $X((n+d_n)T_s)$ can be obtained by the integration of type (5). $i_{ref}=I_{ref}\times\sin(2\pi ft)$ and $u_{grid}=U_m\times\sin(2\pi ft)$ are sinusoidal signal, which change with t, so the system is time-varying system. Quasi-static theory is that, if f is far less than f_s, u_{grid} and i_{ref} are considered as constants during the integration procedure [4]. Therefore, $u_{grid}(n)$ and $i_{ref}(n)$ of the (n)th T_s are

$$\begin{cases} u_{grid}(n) = U_m \times \sin(2\pi f n T_s) \\ i_{ref}(n) = I_{ref} \times \sin(2\pi f n T_s) \end{cases} \tag{7}$$

Based on the quasi-static theory and stroboscopic map criterion, when $nT_s \le t \le (n+d_n)T_s$, the system works at mode 1, the iteration relations of $X(nT_s)$ and $X((n+d_n)T_s)$ is

$$\begin{aligned} X((n+d_n)T_s) &= e^{Ad_nT_s}X(nT_s) + \int_{nT_s}^{(n+d_n)T_s} e^{A((n+d_n)T_s-\tau)}B_1U\,d\tau \\ &= e^{Ad_nT_s}X(nT_s) + A^{-1}(e^{Ad_nT_s}-I)B_1U \end{aligned} \tag{8}$$

Where d_n is the duty ratio of the (n)th T_s.

Similarly, when $(n+d_n)T_s \le t \le (n+1)T_s$, the system works at mode 2. L_1 and L_2 are discharged, and i falls. The iteration relations of $X((n+d_n)T_s)$ and $X((n+1)T_s)$ is

$$\begin{aligned} X((n+1)T_s) &= e^{A(1-d_n)T_s}X((n+d_n)T_s) + \int_{(n+d_n)T_s}^{(n+1)T_s} e^{A((n+1)T_s-\tau)}B_2U\,d\tau \\ &= e^{A(1-d_n)T_s}X((n+d_n)T_s) + A^{-1}(e^{A(1-d_n)T_s}-I)B_2U \end{aligned} \tag{9}$$

Substituting type (10) into type (11), when $i>0$, the discrete model of state variable i in a T_s is

$$X((n+1)T_s) = e^{AT_s}X(nT_s) + (e^{A(n+1)T_s}M_1 + M_2)U \tag{10}$$

Where

$$M_1 = A^{-1}(e^{Ad_nT_s} - I)B_1 \qquad M_2 = A^{-1}(e^{A(1-d_n)T_s} - I)B_2 \tag{11}$$

Substituting the circuit element parameters, type (12) can be rewritten as

$$\begin{aligned} i_{n+1} = {} & e^{-\frac{T_s}{\beta}}i_n - 0.5\alpha(e^{-\frac{T_s}{\beta}} - e^{(d_n-1)\times\frac{T_s}{\beta}}) + e^{-\frac{T_s}{\beta}}(1 - e^{d_n\times\frac{T_s}{\beta}})/(2R) \\ & + U_m \times sin(2\pi\, fnT_s)(e^{-(1-d_n)\times\frac{T_s}{\beta}} - 1)/(2R) \end{aligned} \tag{12}$$

Where $\alpha=E/R$, $\beta=L/R$.

Similarly, when $i<0$ and $nT_s \le t \le (n+d_n)T_s$, the system works at mode 3. When $(n+d_n)T_s \le t \le (n+1)T_s$, the system works at mode 4. The discrete model of state variable i is

$$i_{n+1}=e^{-\frac{T_s}{\beta}}i_n+0.5\alpha(e^{-\frac{T_s}{\beta}}-e^{(d_n-1)\times\frac{T_s}{\beta}})+e^{-\frac{T_s}{\beta}}(1-e^{d_n\times\frac{T_s}{\beta}})/(2R)$$
$$+U_m\times sin(2\pi fnT_s)(e^{-(1-d_n)\times\frac{T_s}{\beta}}-1)/(2R) \quad (13)$$

From Figure. 1, d_n can be expressed as the type (16) in the SMC inverter [6].

$$d_n=\begin{cases}-\varepsilon\times\text{sign}(i_{ref}(n)-i(n))-k_p\times(i_{ref}(n)-i(n)) & (i(n)\geq 0)\\ -\varepsilon\times\text{sign}(i(n)-i_{ref}(n))-k_p\times(i(n)-i_{ref}(n)) & (i(n)<0)\end{cases} \quad (14)$$

d_n satisfies the saturating characteristic.

$$d_n=\begin{cases}0 & (d_n\leq 0)\\ d_n & (0<d_n<1)\\ 1 & (d_n\geq 1)\end{cases} \quad (15)$$

Types (14)～(17) form the discrete-model of the system.

3. State-mutation analysis

3.1. State-mutation phenomenon

Folded diagram and circuit simulation are employed by choosing different ε. N is the number of sampling points of folded diagram in each sinusoidal period, where $N=f_s/f=100$. Other circuit parameters are listed in Table 2.

Table 2. Circuit parameters

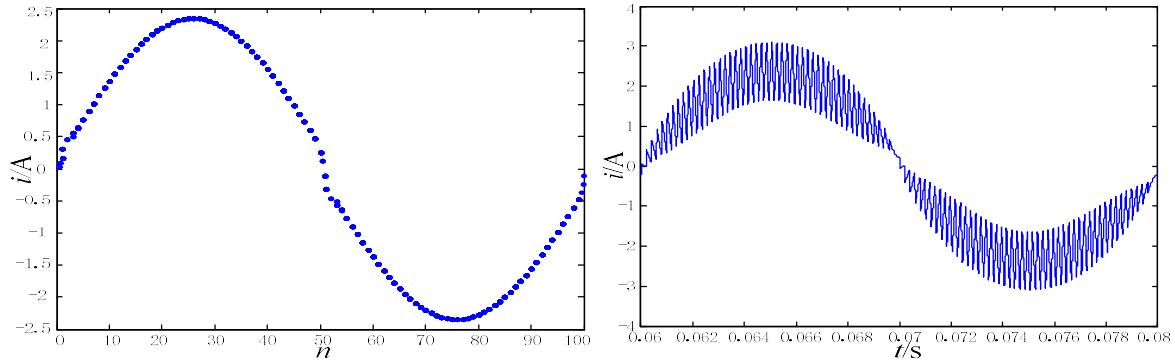
parameters	value	parameters	value
E/V	400	I_{ref}/A	5
$R_1=R_2$/Ω	6	k_p	0.2
$L_1=L_2$/mH	6.85	ε	0.1～0.5

When ε=0.1, folded diagram and circuit simulation of i are shown in Figures. 4(a)-(b). From Figure. 4(a), every sampling point comes to the same point. From Figure. 4(b), the frequency of i is 50Hz, and ripple cycle of i is stable.

When ε=0.3, folded diagram and circuit simulation of i are shown in Figures. 5(a)-(d). From Figure. 5(a), when n=42, folded diagram changes from one point to two points, and from Figure. 5(b), bifurcation-instability phenomenon appears in falling edge at the half-positive period of i. Ripple cycle of i is in stable period-1 when the switching cycles are from $(N_0)T_s$ to $(N_0+16)T_s$, and appears in unstable period-2 at the (N_0+16+1)th T_s firstly, where $N_0=N/4=25$. Therefore, the state-mutation switching cycles is the (42)th T_s. From Figure. 5(c), the period-doubling phenomenon happens at the time when i is near zero point, and near the crest, inductor current i is in steady working condition. Likewise, small amount of $f_s/2$ is observed from the spectrum. Figure. 6(d) is the magnifying Figure of the dotted box in Figure. 6(c). From Figure. 6(d), the period-doubling phenomenon appear at the (17)th T_s firstly, beginning with $\pi/2$.

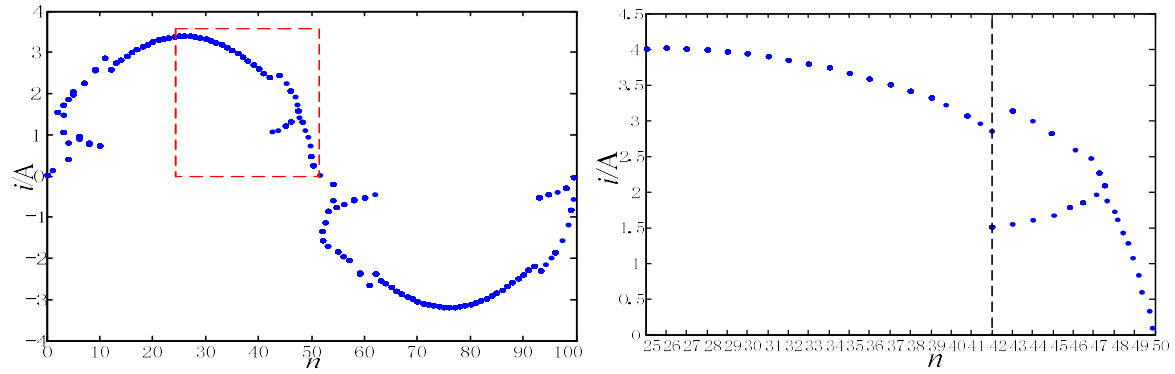
When ε=0.4, folded diagram and circuit simulation of i are shown in Figures. 6(a)-(d). From Figure. 6(a) and Figure. 6(b), state-mutation phenomenon also takes place in this situation. The analyses of ε=0.4 is like that of ε=0.3, state-mutation switching cycles is n=39 in falling edge at the half-positive

period. Meanwhile, from Figure. 5(d), experimental results show that the state-mutation switching cycles are N_0+13+1=39.

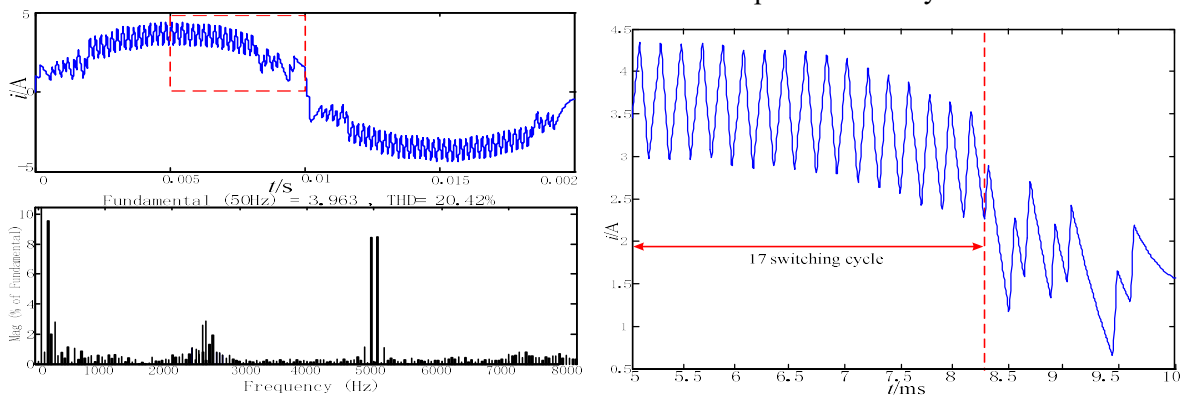


(a) Folded diagram of i for ε=0.1 (b) Time-domain waveform of i for ε=0.1

Figure 4. Steady-state numerical and circuit simulation

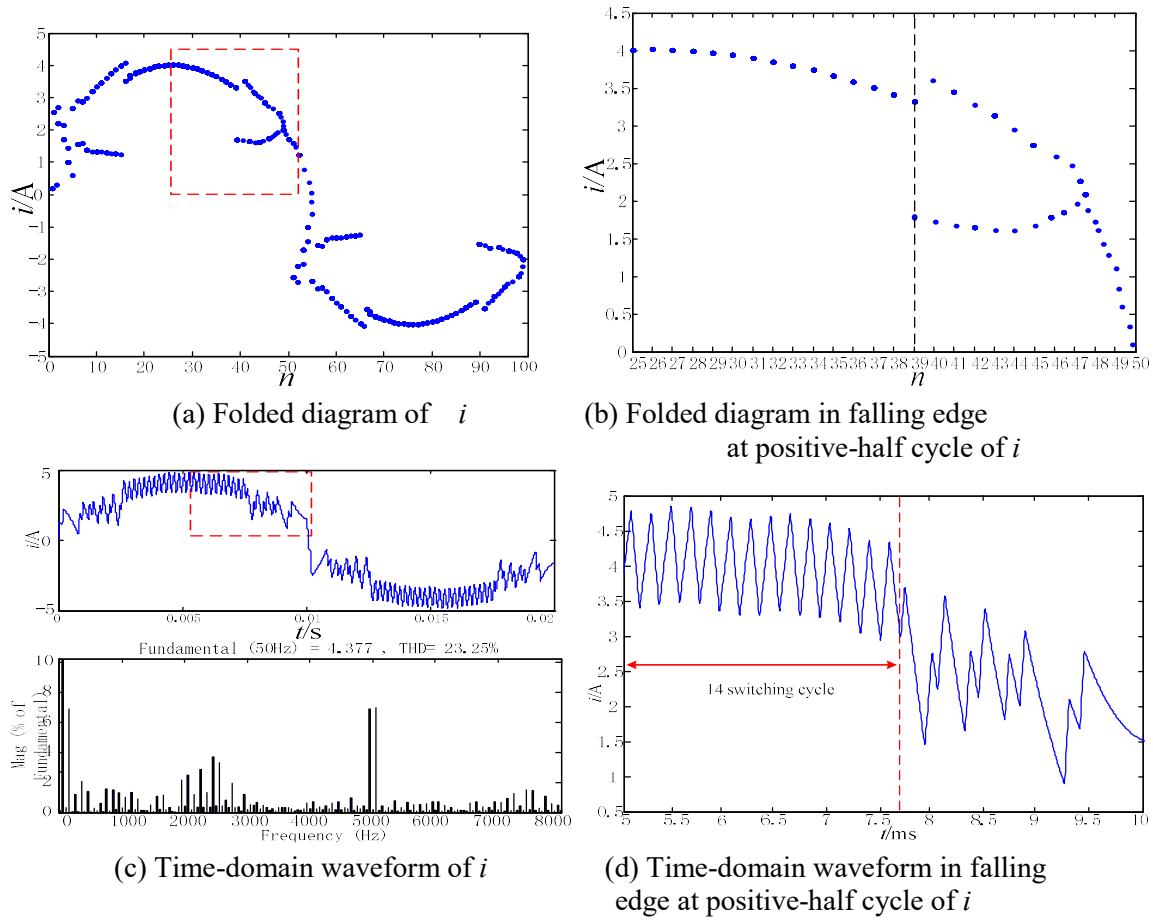


(a) Folded diagram of i (b) Folded diagram in falling edge at positive-half cycle of i



(c) Time-domain waveform of i (d) Time-domain waveform in falling edge at positive-half cycle of i

Figure. 5 State-mutation circuit simulation for ε=0.3



(a) Folded diagram of i

(b) Folded diagram in falling edge at positive-half cycle of i

(c) Time-domain waveform of i

(d) Time-domain waveform in falling edge at positive-half cycle of i

Figure 6. State-mutation circuit simulation for ε=0.4

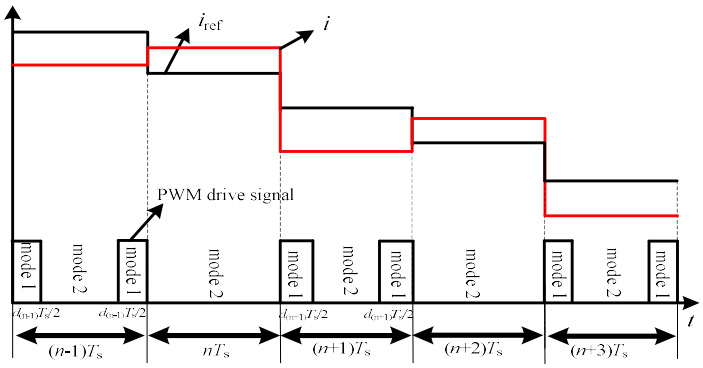
3.2. Cause analysis of state-mutation

To explore the cause of state-mutation phenomenon, PWM driver signals, i_{ref} and i, $u_{carrier}$ and $u_{control}$, size of the duty ratio d_n of 5 consecutive switching cycles are employed in falling edge at positive-half cycle when state-mutation phenomenon appears in the system, which are shown in Figure7(a), Figure 7(b) and Figure 7(c), respectively. On the one hand, when PWM driver signal is high level, the system works at mode 1, L_1 and L_2 are charged. On the other hand, when PWM driver signal is low level, the system works at mode 2, and L_1 and L_2 are discharged. SMC contains symbolic function sign(e), so $u_{control}$ is

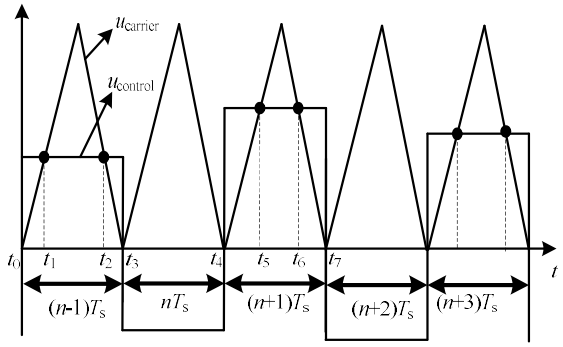
$$u_{\text{control}} = \begin{cases} \varepsilon + k_{\text{p}} \times e & (e > 0) \\ -\varepsilon + k_{\text{p}} \times e & (e < 0) \end{cases} \tag{16}$$

From Figure.7(a), when the system is in steady-state period-1 at the (n-1)th T_s, $i_{ref}(n-1)>i(n-1)$, $e(n-1)=i_{ref}(n-1)-i(n-1)>0$, so $u_{control}(n-1)=\varepsilon+k_p\times e(n-1)>0$. From Figure7(b), $u_{carrier}(n-1)$ and $u_{control}(n-1)$ have two intersections, PWM driver signal jumps twice. The (n-1)th T_s is divided by three stages. From Figure.7(c), if the duty ratio of the (n-1)th T_s is d_{n-1}, $d_{n-1}>0$. PWM driver signal is high at the period t_0-t_1 and t_2-t_3, so the system works at mode 1, L_1 and L_2 are charged. PWM driver signal is low at the period t_1-t_2, the system works at mode 2, L_1 and L_2 are discharged. According to regulator sampling of SPWM, the work-time of t_0-t_1 and t_2-t_3 are $d_{n-1}T_s/2$, the work-time of t_1-t_2 is $(1-d_{n-1})$ T_s. From Figure 7(a), when $i_{ref}(n)<i(n)$ is produced at the (n)th T_s, $e(n)=i_{ref}(n)-i(n)<0$, $u_{control}(n)=-\varepsilon+k_p\times e(n)<0$, so $u_{control}(n)<u_{carrier}(n)$.

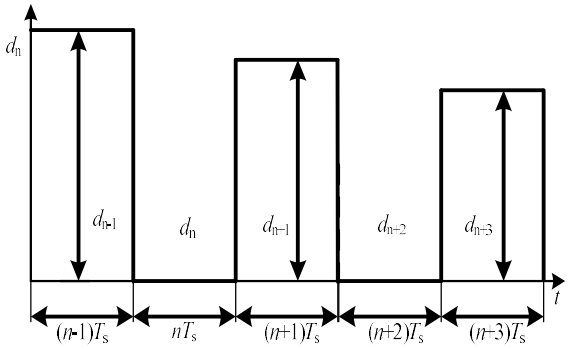
From Figure7(b), $u_{carrier}(n)$ and $u_{control}(n)$ have no intersection, so $d_n=0$, the system works at mode 2. Since hysteresis of the digital control, the change of i lag PWM control signal a T_s. L_1 and L_2 are discharged and i falls sharply at the (n+1)th T_s, $i_{ref}(n+1)>i(n+1)$, $e(n+1)=i_{ref}(n+1)-i(n+1)>0$, $u_{control}(n+1)=\varepsilon+k_p\times e(n+1)>0$. From Figure7(b), $u_{carrier}(n+1)$ and $u_{control}(n+1)$ have two intersections, so $d_{n+1}>0$. Similarly, $d_{n+2}=0$ and $d_{n+3}>0$ can be obtained by the analyses of the (n+2)th T_s and (n+3)th T_s. When the inverter is in steady-stable period-1, switch's duty ratio is monotone by the principle of SPWM inverter [6]-[8]. At the same time, the five switch's duty ratio don't decrease monotonically in falling edge at positive-half cycle, where $d_{n-1}>d_n$, $d_n<d_{n+1}$, $d_{n+1}>d_{n+2}$, $d_{n+2}<d_{n+3}$, the period-doubling bifurcation will appear in the systems.



(a) PWM driver signals, i_{ref} and i



(b) $u_{carrier}$ and $u_{control}$



(c) Size of the duty ratio d_n

Figure 7. Waveforms of the system when bifurcation instability is produced

From the analyses of section 3.1 and section 3.2, it can be seen that the cause of state-mutation phenomenon is that when the error signal is less than zero at a certain T_s, the monotonic decrease of the duty is broken in falling edge at positive-half cycle. Meanwhile, state-mutation switching cycles are different in these two situations, which vary with ε. The variation of state-mutation switching cycle leads it difficult to select sampling switching cycle in the drawing of bifurcation diagram in SMC inverter, because bifurcation diagram of inverter is obtained by sampling several fixed switching cycles of state variables. Thus, the confirmation of state-mutation switching cycle is the key to draw the bifurcation diagram for the SMC inverter. So, it is necessary to explore an innovative judging criterion, which can judge state-mutation switching cycle of i.

4. Judging criterion of state-mutation switching cycle

M switching cycles are selected in falling edge at the half-positive period of i, beginning with N_0. d_n-d_{n+1} divided by $|d_n-d_{n+1}|$ is m, and the algebraic sum of m in M switching cycles is the stability coefficient

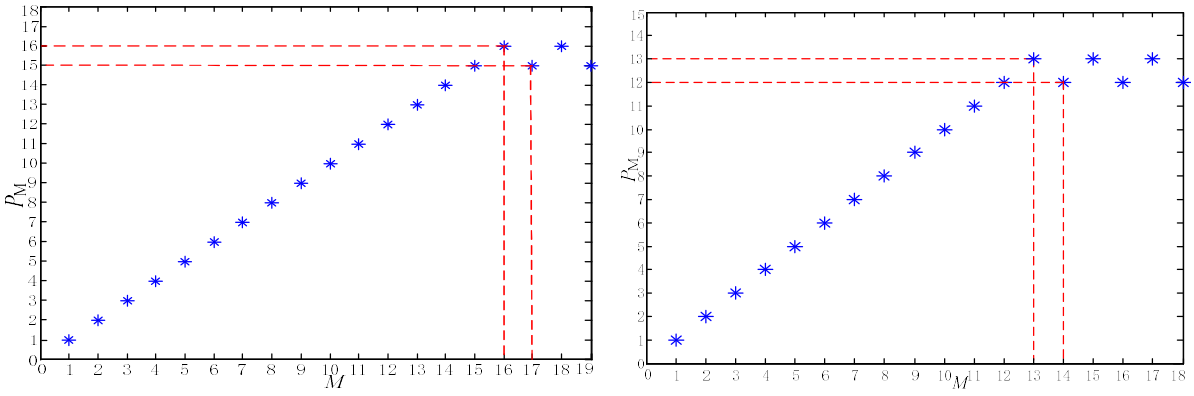
P_M, where d_{n+1}, d_n are the duty ratios of two consecutive switching cycles. Similarly, the P_{M+1} of M+1 switching cycles can also can be obtained. The P_M and P_{M+1} are

$$P_M = \sum_{n=N_0}^{N_0+M-1} \frac{d_n - d_{n+1}}{|d_n - d_{n+1}|} \quad \text{and} \quad P_{M+1} = \sum_{n=N_0}^{N_0+M} \frac{d_n - d_{n+1}}{|d_n - d_{n+1}|} \tag{17}$$

If $P_M=M$ and $P_{M+1}<M+1$, the state-mutation switching cycle can be identified as N_0+M+1.

Testify: The monotonicity of switch's duty ratios can be judged by P_M, and the switching cycles are from $(N_0)T_s$ to $(N_0+M)T_s$. If i changes from period-1 to period-2 at $(N_0+M+1)T_s$ firstly in falling edge at the half-positive period of i, switch's duty ratios monotonically decrease from the $(N_0)T_s$ to $(N_0+M)T_s$ based on the monotonicity of SPWM inverter [2]. So $P_M=M$. Similarly, the monotonicity of switch's duty ratios can be judged by P_{M+1}, and the switching cycles are from $(N_0)T_s$ to $(N_0+M+1)T_s$. If i changes from period-1 to period-2 at $(N_0+M+1)T_s$, the duty ratio of $(N_0+M+1)T_s$ is greater than the duty ratio of $(N_0+M)T_s$, which also can be written as $d_{N0+M+1}>d_{N0+M}$. Substituting $d_{N0+M+1}>d_{N0+M}$ into type (4), $P_{M+1}<M+1$ is obtained.

Validation: When ε=0.3, M=19 and N_0=25, judging result is shown in Figure. 8(a). From Figure. 8(a), when $1\leq M\leq 16$, $P_M=M$. So switch's duty ratios varies monotonically from the $(N_0)T_s$ to $(N_0+16)T_s$. When M=17, P_{17}=15<17. So the (N_0+17)th switch's duty ratio is greater than the (N_0+16)th switch's duty ratio. According to the judging criterion, the state-mutation switching cycle can be identified as $N_0+16+1=42$. So the judging result is agreed to folded diagram and circuit simulation result, which are shown in Figures 7(a)-(b). Analogously, when ε=0.4 and ε=0.5, the judging results are shown in Figure 8a). From Figure 8a and Figure. 8b, the state-mutation switching cycles of ε=0.4 can be analyzed in the same way that are $N_0+13+1=39$, which also are agree to Figure 8.



(a) Judging result for ε=0.3 (b) Judging result of for ε=0.4

Figure 8. Judging results for different SMC parameter ε

5. Experiment

In order to verify the validity of the proposed judging criterion, an experimental

setup is shown Figure 9, which is developed using a DSP model TMS320F2812, IGBT25A-0233 six IGBTs and HFB 16HY20CC two high-performance diodes are used to build the NGCI-H6. Power grid is emulated by Chroma AC source.

Other circuit parameters are listed in Table II. The experimental waveforms of inductor current i are obtained under different parameters ε.

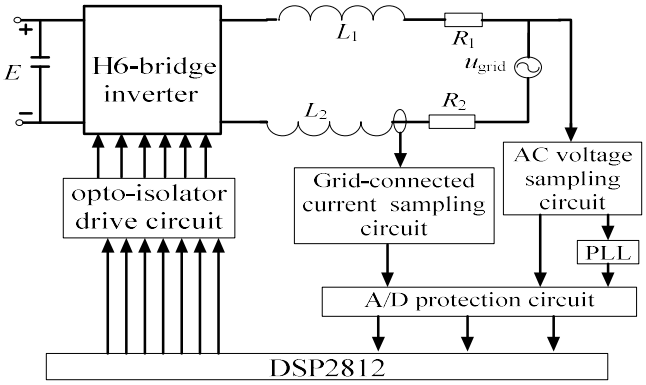
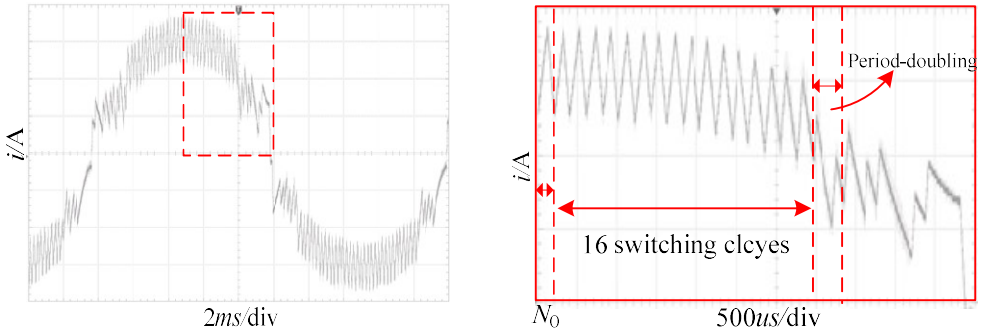


Figure 9. The experimental platform of the NGCI-H6

When ε=0.3 and N_0=2π/4=N/4=25 are employed, experimental results are shown in Figures 10(a)-(b). From Figure 10(a), the frequency of i is 0.02s, it is the same as i_{ref}. The ripple cycle of i appear in bifurcation instability phenomenon at a certain switching cycle, which is agree to circuit simulation that show in Figure 7c). From Figure 10(b), the state-mutation phenomenon appears in falling edge at the half-positive period of i. The cycle of the ripple current is 200us when the switching cycles are from $(N_0)T_s$ to $(N_0+16)T_s$, which is in steady-state period-1. The cycle of the ripple current is 400us, beginning with the (N_0+16+1)th T_s, which is in unstable period-doubling. Therefore, ripple cycle of i is in stable period-1 when the switching cycles are from $(N_0)T_s$ to $(N_0+16)T_s$, and appears in unstable period-doubling at the (N_0+16+1)th T_s firstly in falling edge at the half-positive period. Similarly, when ε=0.4, experimental results are shown in Figures 11(a)-(b).

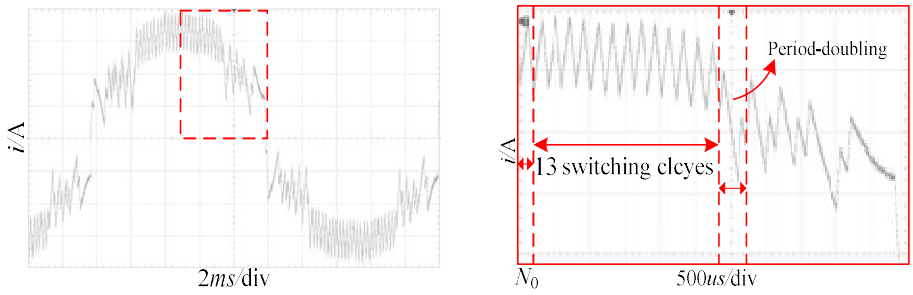
which is equal to the switching cycle T_s. Therefore, the system is in stable period-1, which is consistent with judgment result of the improved SMCNGI-H6 system by criterion of fast-scale stability.



(a) Experimental result of i (b) Experimental result in falling edge at the half-positive period of i

Figure 10. Experimental results of i for ε=0.3

Similarly, when ε=0.4, experimental results are shown in Figures 11(a)-(b). From Figure 11(a), state-mutation phenomenon also takes place in this situation. The analyses of ε=0.4 is similar to that of ε=0.3. From Figure 11(b), state-mutation switching cycles is n=39 in falling edge at the half-positive period. Meanwhile, from Figure 7d), experimental results show that the state-mutation switching cycles are N_0+13+1=39.



(a) Experimental result of *i* (b) Experimental result in falling edge at the half-positive period of *i*

Figure 11. Experimental results of i for ε=0.4

6. Conclusion

A state-mutation phenomenon that the state variables changes from period-1 to period-2 at a certain switching cycle, exists in the SMCNGI-H6 system when a specific ε is selected, and state-mutation switching cycle varies with ε. The new judging criterion can find out the accurate state-mutation switching cycle of the system, which can provide the reference for selecting sampling switching cycle in the drawing of inverter bifurcation diagram. The correctness of judging criterion is proved by folded diagrams and experimental results.

References

[1] Ming, L., Dong, D., Xi, K. M., and Herbert, H. C. I.: 'Slow-Scale and Fast-Scale Instabilities in Voltage-Mode Controlled Full-Bridge Inverter', Circuits, Systems and Signal Processing, vol.27, no.6, pp. 811-831, May 2008.

[2] Xiao, Hua F., Ke Lan, Bin Zhou, Li Zhang, Zaijun Wu: 'A Family of Zero-Current-Transition Transformerless Photovoltaic Grid-Connected Inverter', IEEE Transactions on Power Electronics, vol.30, no.6, pp. 3156-3165, June 2014.

[3] Huai, W., Frede, B., Dan, W., and Bin, Z. : 'Frequency Adaptive Selective Harmonic Control for Grid-Connected Inverters', IEEE Trans. Power Electronics., vol.30, no.7, pp. 3912-3924, Sep 2015.

[4] Nayan, K., Tapas, K.S., and Jayati, D. : 'Sliding Mode Control of PWM Dual Inverter-Based Grid-Connected PV System: Modeling and Performance Analysis', IEEE J. Emerg. Sel. Topics Power Electron., vol.4, no.2, pp.435-444, Dec 2016.

[5] Zhiping Wang, Yunshou Mao, Zhanhu Hu: 'Sliding mode control of uncertain parameter for a matrix rectifier', IEICE Electronics Express , vol.13 , no.12 , pp.20160462, Sep 2016.

[6] Hao, X., Xie, R.L., Yang, X., Liu, T., and Huang, L.: 'Bifurcation and chaos in sliding mode controlled first-order h-bridge inverter based on pulse width modulation', Acta Phys. Sin., vol.62, no. 20, pp. 200503-1-200503-15, Nov 2013.

[7] Wu Chen, Li Yinghui, Lin Mao,Li Zhe: 'Parameters design of a sliding mode controller with a hysteresis band for buck converters in continuous and discontinuous conduction modes', IEICE Electronics Express., Vol.13, No.13 ,pp: 20160448, may 2016.

[8] Liao, Z. X., Luo, X. S., Huang, G, X. : 'Numerical modeling and research on nonlinear dynamic behaviors of two-stage photovoltaic grid-connected inverter', Acta Phys. Sin., vol.64, no.13, pp. 130503-1-130503-7, Aug 2015.